Exploring Space-Radiation Induced Dark Signal and Random-Telegraph-Signal in a Sony IMX219 CMOS Image-Sensor

Aubin Antonsanti[1,4,5], Jean-Marie Lauenstein[2], Alexandre Le Roch[3], Landen Ryder[2],
Cédric Virmontois[4], Vincent Goiffon[5]
[1] Southeastern Universities Research Association at NASA Goddard Space Flight Center (GSFC), USA
[2] NASA Goddard Space Flight Center, USA/ [3]NASA Postdoctoral Program at NASA GSFC, USA
[4] Centre National d'Etudes Spatiales, Toulouse, France/ [5] ISAE-Supaero, Toulouse, France
Email: aubin.antonsanti@isae-supaero.fr

I. Introduction

Beyond high-performance image sensors embedded in telescopes or scientific instruments, additional cameras are required for satellite orientation, Entry Descent Landing (EDL) sequence, and rover navigation. Star trackers, proximity cameras, and engineering cameras are examples of non-scientific imaging systems where the development cost is far smaller than the critical scientific payload and where the use of Commercial-Off-The-Shelf (COTS) CMOS Image Sensors (CISs) is of great interest. Over the past decade, space applications have seen an increasing number of engineering cameras that have not been specifically developed for space applications at first [1]. New needs have arisen to assist missions with high frame rates and fast data transmission where COST CIS camera modules are preferred candidates.

Therefore, implementing COTS CIS in space missions is a trend that is more likely to keep growing as the number of missions increases. All those new applications will drastically increase the need for long-lifetime cameras, making Radiation Hardness Assurance (RHA) way more critical contrary to previous missions. To meet future mission requirements, the radiation-induced performance degradation of COTS CIS is currently being explored on several CIS technologies.

Both Total Ionizing Dose and Displacement Damage Dose lead to a dark current increase altering the dynamic range as well as creating hot pixels altering the image quality. Some pixels also exhibit a dark current Random Telegraph Signal (DC-RTS), seen as blinking pixels with a time constant in the range of a few seconds, minutes, hours [2], [3]. Such pixels see their dark current randomly and instantaneously switch between two or more discrete dark current levels preventing in-flight calibration and perturbing the normal operation.

This work aims at exploring radiation-induced dark signal and Dark Current Random-Telegraph-Signal in a COTS, micro-meter pitch, backside-illuminated (BSI) CMOS Image Sensor (CIS).

II. Device Information

The device under test (DUT) is a Sony IMX219. The IMX219 is a backside illuminated CIS with 3280 × 2464 pixels and 1.12 μm pitch. The detection layer of the sensor is stacked on another silicon die containing the sensor's ROIC and logic electronics. A Scanning Electron Microscopy (SEM) cross-section is shown in Fig. 1 with the different layers of the optical stack identified. Pixels are arranged in a clover leaf patter [4] where a subgroup of four pinned-photodiodes (PPDs) are connected through Transfer Gates (TG) to a shared Sense-Node (SN). Two subgroups are sharing the same reset (RST) and row select (SEL) transistors. This pattern is commonly employed and allows to use 11 transistors for 8 pixels (1.375 transistors per pixel) as seen in Fig. 2.

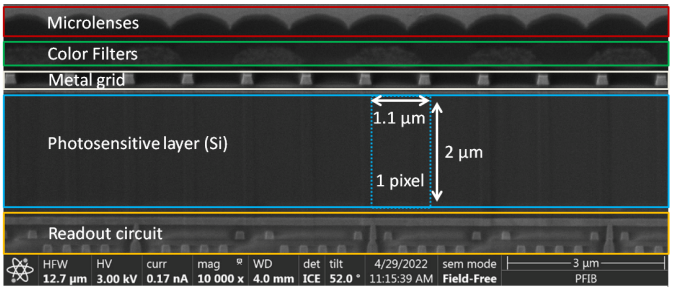

Fig. 1. SEM image of the IMX219 optical stack's cross-section

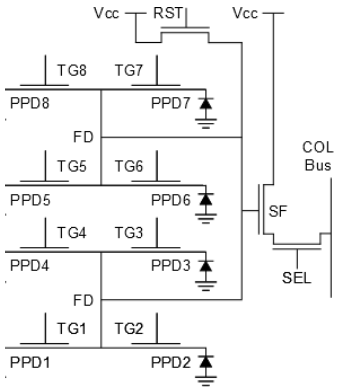

Fig. 2. IMX219 pixels electrical layout

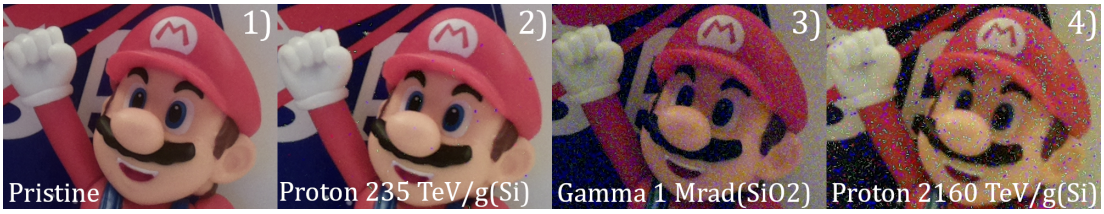

Fig. 3. Images taken with an integration time of 400ms and unitary gain with a 1) pristine; 2) 235 TeV/g(Si) proton irradiated; 3) 1 Mrad(SiO2) gamma irradiated; 4) 2160TeV/g(Si) irradiated IMX219.

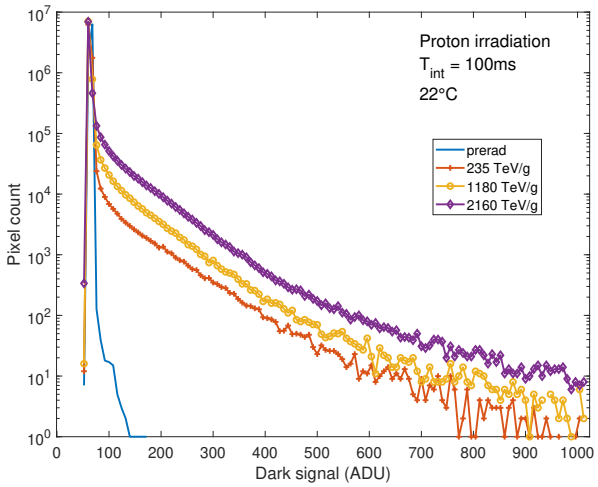

Fig. 4. Histograms of dark signal of proton irradiated IMX219. Proton induced Displacement Damage is responsible for the creation of a tail of hot pixels whose occurrence increases with the total dose.

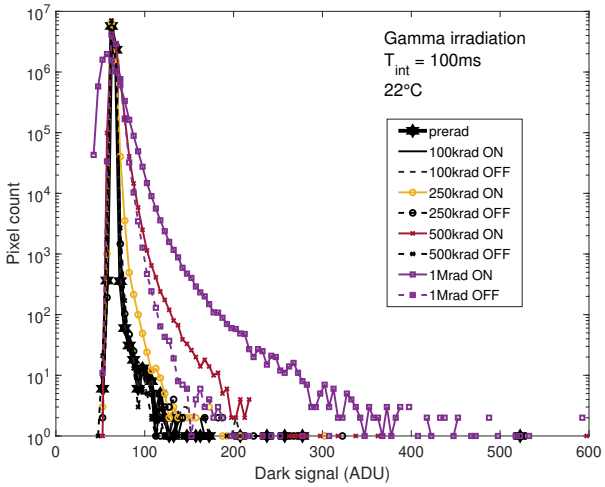

Fig. 5. Histograms of the dark signal of gamma irradiated IMX219. Ionizing radiations are responsible for the widening of the dark signal distributions. The fact that the main occurrence peak isn't shifting towards the high ADU values shows the effect of the on-chip black clamping circuit.

III. Irradiation Details

Two irradiation campaigns have been made. The first used a 62 MeV proton beam at the Light Ion Facility (LIF) located in Université Catholique de Louvain, Belgium. All DUTs were grounded during irradiation at room temperature. The deposited Displacement Damage Dose (DDD) ranged from 235 to 2160 TeV/g (Si). The second used gamma rays at the Radiation-Effect-Facility of the NASA Goddard Space Flight Center. Both grounded and biased DUTs were used and irradiated at room temperature. A thermocouple was used to monitor the temperature of the biased DUT during irradiation. Devices were heating up to 32°C when biased but irradiation didn't cause extra heating. The deposited Total Ionizing Dose (TID) ranges from 10 $\mathrm{krad(SiO_2)}$ to 1 $\mathrm{krad(SiO_2)}$.

All measurements were performed in a climatic chamber whose temperature was set so that the temperature of the DUTs was 22°C when biased.

IV. Results

A. Dark current degradation

Proton-induced displacement damages are responsible for the creation of an exponential dark current tail of hot pixels as seen in Fig. 4 and reported multiple times in previous studies on CIS radiation hardness [5]–[9]. In [5], it was shown that the displacement damage induced dark current degradation on the DUT was following the typical trend with the dose for CIS.

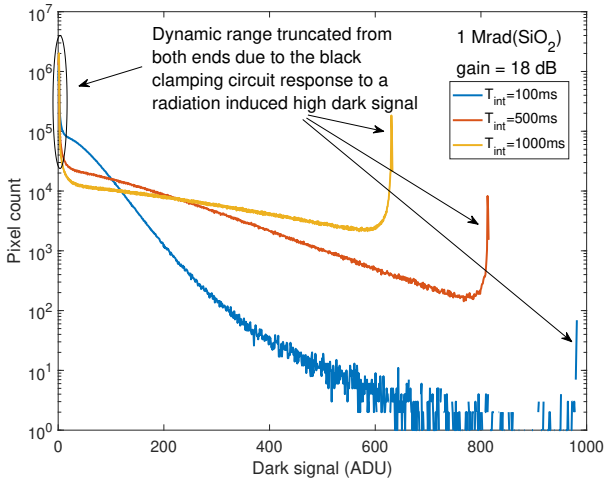

Fig. 6. Effects of the black-clamping circuit on the dynamic range at high TID. The signal histogram is shifted towards low ADU values to compensate for the radiation induced dark signal which significantly increases with the integration time. The correction forces pixels' value to 0 ADU and the saturation level is also reduced, thus diminishing the 10-bit ADC initial dynamic range.

TABLE I
IMX219 DSNU AND READOUT NOISE

Particle	Bias	Dose $\mathrm{krad(SiO_2)}$	DSNU %	Readout noise ADU RMS
ref	-	-	0.66	2.03
γ	gnd	100	0.64	2.03
γ	gnd	250	0.92	2.08
γ	gnd	500	1.39	2.04
γ	gnd	1000	6.23	2.08
γ	on	100	0.78	2.08
γ	on	250	2.06	1.59
γ	on	500	5.72	1.82
γ	on	1000	14.8	2.2
		$\mathrm{TeV/g(Si)}$		
ref	-	-	0.59	1.87
p^+	gnd	235(10 krad)	18.0	2.1
p^+	gnd	1180(50 krad)	37.7	2.27
p^+	gnd	2160(90 krad)	43.3	3.27

However, the study concluded that no TID induced degradation was observed although devices were irradiated up to a TID of $90\,\mathrm{krad(SiO_2)}$.

Fig. 5, displays histograms of dark signal for gamma irradiated devices. It can be seen that there are no obvious changes in the histogram shape bellow $250\,\mathrm{krad(SiO_2)}$ for the biased devices versus bellow $1\,\mathrm{Mrad(SiO_2)}$ for the grounded devices. Above these values, histograms widen with dose, reflecting an increase in the dark current shot-noise. The increase in dark current mean value should be visible in the form of a shift of the peak of maximum occurrence towards high dark signal values. Such a shift isn't visible here due to the sensor's black clamping circuit that shifts the output histogram so that the mean dark signal is coded 64 ADUs. This mean dark signal is evaluated using 16 rows of optically black pixels.

Table I sums up the measured Dark Signal Non Uniformity (DSNU) and readout noise for both the proton and gamma irradiations. The DSNU was evaluated as the standard-deviation of the pixels' dark signal over the array divided by the mean dark signal using an integration time of 100 ms. The readout noise was evaluated as the average standard deviation of individual pixel's dark signal values over 100 frames using an integration time of 100 ms. It can be seen that the DSNU is much lower for the gamma irradiated devices than for the proton irradiated device. This is an expected result since the TID induces an homogeneous degradation of the dark current over the array while DDD will create individual hot pixels [7]. This effect can also be seen on the pictures in Fig. 3.

Although the black clamping can mitigate part of the dark current degradation, the dynamic range of the sensor is still reduced by the increase of the dark current level and shot-noise. As seen in Fig. 6, at high dose and in some specific use cases (low luminosity, high integration time, high gain), the radiation induced dark signal increase will cause the black clamping circuit to shift a lot of the histogram values to 0 ADU and will also reduce the saturation level bellow the maximum value that the 10 bit ADC can code, 1023.

B. Dark current Random Telegraph Signal

Fig. 7 displays an example of the temporal response of an RTS pixel. An edge-detection algorithm [10] allows to extract

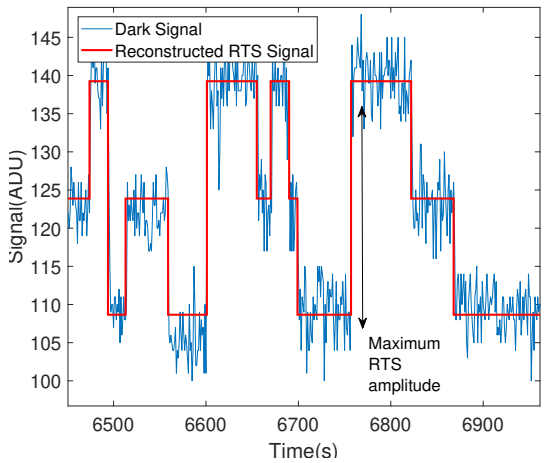

Fig. 7. Temporal evolution of the dark signal of a pixel exhibiting 3 RTS levels. The maximum RTS amplitude is the highest jump between two consecutive discrete levels. All RTS measurements were carried out using an integration time of 100ms and an inter-sample time of 1s. RTS traces are extracted using a sharp edge detection algorithm [10].

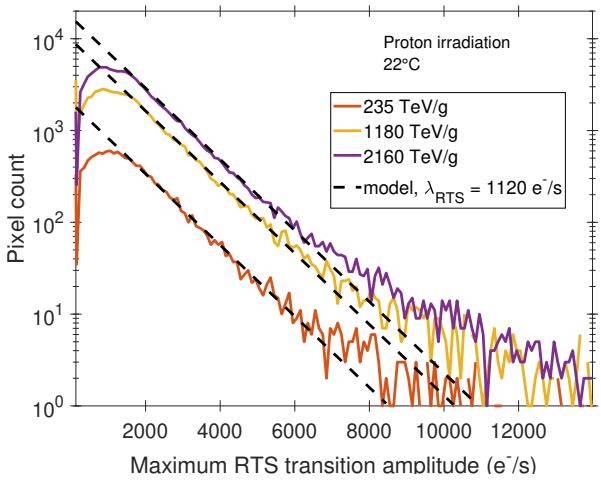

Fig. 8. RTS Maximum transition amplitude histograms of proton irradiated IMX219. The number of pixel exhibiting an RTS behavior increases with the dose. The slope of these exponential distributions is the mean maximum RTS transition amplitude. A slope of 1120 e-/s is found, close to the 1200 e-/s reported in the literature [7] [11].

TABLE II
IMX219 RTS DETECTION

Particle	Bias	Dose $\mathrm{krad(SiO_2)}$	RTS Fraction %	%Multi-level %
γ	gnd	100	0	-
γ	gnd	250	0	-
γ	gnd	500	0.16	0
γ	gnd	1000	2.93	0.94
γ	on	100	0.01	0
γ	on	250	0.99	1.0
γ	on	500	16.2	3.8
γ	on	1000	32.8	9.5
		$\mathrm{TeV/g(Si)}$		
p^+	gnd	235(10 krad)	0.64	23.6
p^+	gnd	1180(50 krad)	3.18	27.1
p^+	gnd	2160(90 krad)	5.14	25

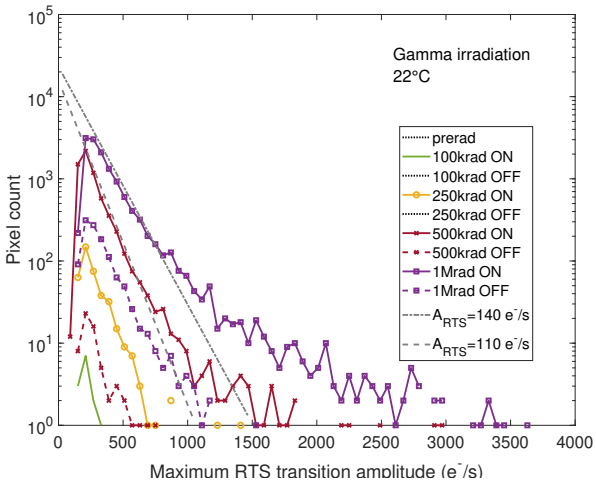

Fig. 9. RTS Maximum transition amplitude histograms of gamma irradiated IMX219. Black dots in the legend indicate dose steps where no RTS pixels where detected. Biasing the device during irradiation strongly increases the number of RTS pixels created.

the highest transition between two levels, the number of RTS level as well as the number of transitions. Black-clamping is not an issue when extracting RTS amplitudes as it can be seen as an offset that should not vary from frame to frame. Prerad RTS detection revealed less than 4 RTS pixels per milion pixel.

Proton-induced RTS maximum transition amplitudes are exponentially distributed (Fig. 8). The experimental RTS maximum transition amplitude distributions' associated exponential slopes values are well in line with the values found in the literature ($A_{\mathrm{RTS}} \approx 1200$ e-/s at $\approx 22\,^{\circ}\mathrm{C}$) for a wide range of image sensor technology nodes, designs, or pixel size [5], [10], [11]. This result strengthens the idea of a universal behavior of displacement damage-induced RTS in silicon.

Table II shows the fraction of RTS pixels detected and the fraction of RTS pixels exhibiting more than two RTS levels after the different irradiations. For the proton irradiations, it has been shown in [5] that both quantities were significantly smaller in the DUT than in CIS with a larger pitch. This reduction of the fraction of RTS and of multilevel RTS has been directly linked to the reduction of the pixels' sensitive volume.

For the TID induced RTS pixels after gamma irradiation, it can be seen in Fig 9 that the maximum RTS amplitudes are mostly exponentially distributed and of a much lower than the displacement damage induced RTS pixels. The exponential slope of ≈ 110e-/s matches the literature [7].

Both proton and gamma induced maximum RTS amplitudes histograms deviate from the exponential behavior at high dose. This is not a commonly reported result and local Electric-Field-Enhancement was proposed in [5] as a phenomenon that could explain this deviation.

Table II also shows that the fraction of RTS pixel increases faster when the device is biased during gamma irradiation. For the biased devices, the creation of RTS pixels accelerates significantly after $250\mathrm{krad}(\mathrm{SiO_2})$. It can be seen that, comparatively to displacement damage induced RTS pixels, TID induced RTS pixels are mostly exhibiting two RTS levels.

V. Conclusions

Proton irradiations showed that the DUT was following the typical trend for dark-current and RTS degradation for CIS. The reduced pixel pitch induced a decrease of the fraction of pixels disclosing an RTS behavior when comparing to larger pitch CIS.

Gamma irradiations revealed that the DUT has a very good tolerance to TID up to 250 krad. Biasing the DUT during irradiation has a strong negative impact on the TID induced degradation of both the dark signal and RTS behavior.

A deviation of the maximum RTS transition amplitude distributions from a purely exponential behavior is observed in both the proton and gamma irradiations. Local Electric-Field-Enhancement was proposed as a first hypothesis on the origin of this behavior in [5], due to an observed shift of the RTS amplitudes activation energies from the mid-gap. The increase in dopants gradient profiles resulting from the submicrometer pixel pitch reduction trend imposed by the smartphone camera market is also supporting this hypothesis [12].

The response to cumulative dose of the IMX219 is very promising for a use as an engineering/proximity camera in space applications, where the dose rarely exceed the 100 krad range. Cumulative dose might however not been the most challenging aspect in assessing the radiation hardness of such 3D-stacked CIS. The device susceptibility to Single-Event-Effects; such as transistor latchup or functional interrupt; might be the real bottleneck because of the presence of the ROIC and logical die stacked under the detection layer.

References

[1] J. Maki *et al.*, "The Mars 2020 Engineering Cameras and microphone on the perseverance rover: A next-generation imaging system for Mars exploration," *Space Sci. Rev.*, vol. 216, pp. 1–48, Nov. 2020.

[2] I. H. Hopkins and G. R. Hopkinson, "Random telegraph signals from proton-irradiated CCDs," *IEEE Trans. Nucl. Sci.*, vol. 40, no. 6, pp. 1567–1574, Dec. 1993.

[3] I. Hopkins and G. Hopkinson, "Further measurements of random telegraph signals in proton irradiated CCDs," *IEEE Trans. Nucl. Sci.*, vol. 42, no. 6, pp. 2074–2081, Dec. 1995.

[4] E. R. Fossum and D. B. Hondongwa, "A review of the pinned photodiode for CCD and CMOS image sensors," *IEEE J. Electron Devices Soc.*, vol. 2, no. 3, pp. 33–43, May 2014.

[5] A. Antonsanti *et al.*, "Probing dark current random telegraph signal in a small pitch vertically pinned photodiode cmos image sensor after proton irradiation," *IEEE Transactions on Nuclear Science*, vol. 69, no. 7, pp. 1506–1514, 2022.

[6] J.-M. Belloir *et al.*, "Pixel pitch and particle energy influence on the dark current distribution of neutron irradiated CMOS image sensors," *Opt. Express*, vol. 24, no. 4, pp. 4299–4315, Feb. 2016.

[7] V. Goiffon, "Radiation effects on CMOS active pixel image sensors," in *Ionizing Radiation Effects in Electronics: From Memories to Imagers.* Boca Raton, FL, USA: CRC Press, 2015, pp. 295–332.

[8] C. Virmontois, V. Goiffon *et al.*, "Similarities between proton and neutron induced dark current distribution in CMOS image sensors," *IEEE Trans. Nucl. Sci.*, vol. 59, no. 4, pp. 927–936, Aug. 2012.

[9] C. Virmontois *et al.*, "Dark current random telegraph signals in solid-state image sensors," *IEEE Transactions on Nuclear Science*, vol. 60, no. 6, pp. 4323–4331, 2013.

[10] V. Goiffon, G. R. Hopkinson *et al.*, "Multilevel RTS in proton irradiated CMOS image sensors manufactured in a deep submicron technology," *IEEE Trans. Nucl. Sci.*, vol. 56, no. 4, pp. 2132–2141, Aug. 2009.

[11] C. Virmontois *et al.*, "Dark Current Random Telegraph Signals in Solid-State Image Sensors," *IEEE Trans. Nucl. Sci.*, vol. 60, no. 6, pp. 4323–4331, Dec. 2013.

[12] M. Uchiyama *et al.*, "A 40/22nm 200mp Stacked CMOS Image Sensor with 0.61um Pixel," in *2021 International Image Sensor Workshop (IISW)*, Online Conference, 20-23 Sept 2021, Art. no. R02.